Nanoscale

PAPER

View Article Online
View Journal | View Issue

Cite this: *Nanoscale*, 2025, **17**, 2728

Exploration of low-sulfonate lignin electrospinning conditions for the development of new renewable lubricant formulations†

José F. Rubio-Valle, *[a] Concepción Valencia, [a] Gethzemani M. Estrada-Villegas, [b] José E. Martín-Alfonso [a] and José M. Franco [a]

This study explores the preparation of lubricating oleo-dispersions using electrospun nanofibrous mats made from low-sulfonate lignin (LSL) and polycaprolactone (PCL). The rheological and tribological properties of the oleo-dispersions were significantly modulated for the first time through the exploration of LSL/PCL ratio and electrospinning conditions such as applied voltage, distance between the tip and collector, flow rate, ambient humidity, and collector configuration. Adequate uniform ultrathin fibers and Small-amplitude oscillatory shear (SAOS) functions of the oleo-dispersions, with storage modulus values ranging from 10^2 to 10^5 Pa at 25 °C, were obtained with a flow rate of 0.5 ml h^{-1}, an applied voltage of 15 kV, relative humidity 45% and a static collector. The LSL/PCL ratio directly affected the mechanical properties of the membranes, influencing stiffness and wear resistance. Higher PCL content enhanced membrane stiffness, reflected in increased SAOS values, but also led to higher friction coefficients (from 0.11 to 0.18) and more pronounced wear traces (measured by wear diameter: 440 to 860 μm). These interactions underscore the complex relationship between micro- and/or nano-structures and tribological performance. This study establishes a clear link between electrospinning conditions and the performance of oleo-dispersions, offering a versatile platform for the development of customizable, renewable lubricants. These findings contribute to the advancement of sustainable lubrication technologies, demonstrating the potential of tailor-made oleo-dispersions as alternatives to traditional lubricants.

Received 25th October 2024,
Accepted 10th January 2025

DOI: 10.1039/d4nr04426f

rsc.li/nanoscale

1. Introduction

In recent decades, various strategies have been implemented to promote a more sustainable use of renewable resources.[1,2] These policies aim to manage natural resources more responsibly, reduce dependence on non-renewable energy sources and mitigate the effects of climate change.[3,4] In this context, the bioeconomy has emerged as an economic model that integrates terrestrial, marine and waste biological resources into sustainable industrial practices, responding to the urgent need to protect the environment and address the growing scarcity of oil.[5,6] This approach seeks not only environmental benefits, but also economic and social impacts, in line with the principles of the triple bottom line.[7] As a result, the scientific community has been exploring more sustainable solutions in various industries.[8–10]

In the field of lubrication, approximately 55% of the volume of lubricants marketed each year contributes to environmental pollution.[11] This is due to the complexity of conventional formulations, which predominantly use mineral or non-biodegradable synthetic oils together with thickeners such as lithium and calcium soaps.[12–14] The key properties of lubricating greases, generally classified by their consistency in NLGI grades, depend on the microstructure created by the thickeners and concentrations used.[15] The integration of bioeconomic approaches into lubricant technology aims not only to reduce dependence on non-renewable resources, but also to mitigate the environmental impacts associated with their production, consumption and waste management.[16,17]

The search for sustainable thickening or structuring agents for oily media has been the subject of increasing research.[18–20] However, compatibility between biopolymers and vegetable oils often requires chemical modifications – such as acetyl-

[a]*Pro2TecS – Chemical Product and Process Technology Research Center. Department of Chemical Engineering and Materials Science. Universidad de Huelva. ETSI, Campus de "El Carmen", 21071 Huelva, Spain.*
E-mail: josefernando.rubio@diq.uhu.es
[b]*CONACYT-Centro de Investigación en Química Aplicada, Parque de Innovación e Investigación Tecnológica (PIIT), Apodaca 66628, Mexico*

† Electronic supplementary information (ESI) available. See DOI: https://doi.org/10.1039/d4nr04426f

ation, ethylation or acylation – to improve their performance and stability in lubricant applications.[21–23] Although these systems are bio-based and non-toxic, the production processes involve complex reactions and the use of unsustainable solvents, underscoring the need to develop cleaner and more efficient alternative methods that minimize or eliminate chemical modifications.

A promising alternative is to improve the compatibility of biopolymers with oils through physical interactions.[24,25] The hypothesis behind this approach is that a structure consisting of micro- or nano-sized fibers, with high porosity and surface-to-volume ratio, could facilitate the creation of a three-dimensional percolation network within the oil medium.[26,27] In the field of nanofabrication, electrospinning stands out for its industrial scalability and its ability to modify fiber morphology.[28,29] In this regard, the physicochemical properties of the solutions (viscosity, surface tension and electrical conductivity) and the conditions of the electrospinning process play an essential role.[30,31] This process is closely related to the electric field generated by both the applied voltage and the free and induced charges on the jet surface.[32] In addition, these external conditions and parameters significantly influence the diameter and morphology of the nanofibers.[33,34] It is possible to control the electric field between the needle tip and the collector by adjusting parameters such as the applied voltage, the distance between the needle and the collector, the type of collector and the needle diameter.[35–37] All these factors are considered under the category of processing conditions. These conditions include environmental parameters such as temperature and relative humidity, which are controlled within the electrospinning chamber.[38,39] Numerous studies have correlated electrospinning conditions with nanofiber morphological properties.[40] In particular, Deitzel *et al.*[41] performed a systematic evaluation of the effects of spinning voltage and spinning solution concentration on the morphology of the formed nanofibers, providing a detailed understanding of how these parameters influence the final structure.

Among the potential materials for electrospinning, lignin stands out as a promising candidate due to its abundance as the second most abundant natural macromolecule in nature after cellulose.[42,43] Derived mainly as a waste and/or by-product of the paper industry and biofuel production, lignin not only reduces dependence on fossil fuels, but also promotes sustainability by extending the life cycle of these materials.[44,45] However, the electrospinning of lignin presents challenges, primarily due to its rigid structure and irregular molecular weight distribution, which hinder the jet-stretching process required for fiber formation.[46,47] These intrinsic characteristics of lignin, rather than its molecular weight alone, make it difficult to form continuous fibers. To address these limitations, it is common to use dopant polymers that increase the entanglement density in lignin solutions, thereby improving their ability to form fibers.[48–50] In addition to using dopant polymers, selecting the appropriate type of lignin can significantly influence the electrospinning process.[50–52] Low-sulfonate lignin (LSL), for instance, offers advantages over other technical lignins, such as Kraft or organosolv lignin, due to its sulfonate groups ($-SO_3H$), which enhance its solubility and compatibility with solvents.[53] These properties facilitate the preparation of homogeneous spinning solutions, a crucial factor for successful fiber formation.[54,55] When combined with dopant polymers like polycaprolactone (PCL)—known for its biodegradability, biocompatibility, and high electrospinnability—LSL provides a versatile platform for overcoming the inherent challenges of electrospinning lignin.[25,56] While the presence of sulfur in LSL may raise concerns about the formation of corrosive by-products, the low sulfonate content of LSL significantly reduces these risks compared to other more sulfonated lignins. This aspect is particularly relevant in the lubricant sector, where there is increasing regulatory pressure to limit the sulfur content in formulations due to its potential to generate corrosive by-products and environmental challenges.[57,58]

In this work, PCL-doped LSL electrospun nanostructures with different morphologies were evaluated as a structuring agent in a vegetable oil. For the first time, it was investigated how key electrospinning parameters of LSL/PCL solutions can modulate the structuring ability of the electrospun nanostructure in the oil medium. For this purpose, rheological analyses of the oil dispersions were performed and correlated with the morphological properties of the electrospun mats. The results presented here demonstrate the potential of LSL/PCL micro and/or nanofibers to replace traditional thickeners in the lubricant industry, thus contributing to the creation of renewable, more sustainable and efficient lubricants.

2. Results and discussion

2.1. Influence of electrospinning conditions on the morphological properties of nanostructures

Electrospinning process is intrinsically linked to the experimental conditions used, which directly influence the final morphology of the nanofibers, affecting their diameter, distribution and physical properties,[36,37,59] which are crucial for industrial and biomedical applications.[60–62] In this section, the effects of different electrospinning conditions on the morphological properties of the produced ultrathin fibers were investigated. A series of experiments were performed in which key parameters were analyzed individually, and the results are summarized in Table 1. First, the effect of the needle diameter (G), a determining factor that depends on the viscosity of the solution and provides stability to the solution jet during electrospinning, was studied.[35] The 90LSL-10PCL spinning solution was used in all experiments. The results show that when larger diameter needles are used, the average fiber diameter (D_{AV}) is higher compared to smaller diameter needles such as 21G and 23G. Specifically, the fiber diameter decreased from 0.55 μm with a 19G needle to 0.42 μm with a 23G needle, holding all other process variables constant. This

Table 1 Experimental parameters are used in electrospinning to produce ultrathin fibers. Key variables: needle diameter (*G*), solution flow rate (*Q*), needle-collector distance (*d*), applied voltage (*V*), collector type (Type c), electrospinning configuration (Conf), humidity relative (HR) and average diameter of fibers obtained (D_{AV}). Using 90LSL-10PCL spinning solution

G	*Q* (ml h^{-1})	*d* (cm)	*V* (kV)	Type c (rpm)	Conf.	HR (%)	D_{AV} (μm)
19*G*	0.5	15	15	0	Horizontal		0.55
21*G*						45	0.51
23*G*							0.42
21*G*	0.1	15	15	0	Horizontal		0.29
	0.5					45	0.51
	1						0.54
21*G*	0.5	7	15	0	Horizontal		0.59
		15				45	0.51
		30					0.17
21*G*	0.5	15	7	0	Horizontal		0.58
			15			45	0.51
			30				0.07
21*G*	0.5	15	15	0	Horizontal		0.51
				300		45	0.34
				600			0.19
21*G*	0.5	15	15	0	Horizontal	45	0.51
					Vertical		0.49
						25	0.46
21*G*	0.5	15	15	0	Horizontal	45	0.51
						70	0.35

trend is visualized in the parallel coordinates graph (see Fig. 1c). This behavior is consistent with that reported by other authors who have shown that a larger needle diameter results in a higher solution flow rate from the needle to the collector, thereby increasing the diameter of the fibers formed.[63,64] This is explained by the inverse relationship between flow rate and jet elongation under an electric field, resulting in smaller diameter fibers when smaller gauge needles are used.[35]

Another fundamental parameter in controlling the ultrathin fibers diameter is the flow rate (*Q*), three different flow rates (0.1, 0.5 and 1 ml h^{-1}) were evaluated, keeping the other parameters constant and using the 21*G* needle, since it provided greater heterogeneity in the structure and the D_{AV} was similar to that of the 19*G* needle. The results showed that as the flow rate increased, the average diameter of the fibers also increased from 0.29 μm to 0.54 μm. This effect can be attributed to the increased amount of polymer available for fiber formation as the flow rate increases, resulting in thicker fibers (see Fig. 1c). This phenomenon has been documented in several studies, where a higher flow rate tends to produce thicker fibers due to lower stress in the solution jet, which reduces electric field induced stretching.[65,66] However, it is important to note that an excessively high flow rate can lead to polymer accumulation at the needle tip, which could result in droplet formation or jet instability, compromising the uniformity of the fibers obtained.[67] The distance between the needle and the collector (*d*) is another critical factor affecting fiber morphology, three distances (7 cm, 15 cm and 30 cm) were analyzed under similar experimental conditions. The results show that by reducing the distance to 7 cm, fibers with a larger D_{AV} (0.59 μm) are obtained, while by increasing the distance to 30 cm, the D_{AV} decreases significantly to 0.17 μm. This behavior can be explained by the longer time available for the solution jet to undergo additional stretching under the influence of the electric field when the distance is greater.[33,68] At shorter distances, the stretching time is reduced, resulting in thicker fibers. Previous studies have confirmed this relationship, suggesting that a longer distance favors obtaining thinner fibers due to the greater stretching of the jet before it solidifies upon reaching the collector.[69,70]

The applied voltage (*V*) is a key parameter for the generation of the solution jet in the electrospinning process. The voltage was kept at 15 kV and additional variations were made at 7 kV and 30 kV. It was observed that at 7 kV, the fibers had an D_{AV} of 0.59 μm, while increasing the voltage to 30 kV, the diameter of the fibers decreased to 0.17 μm. This behavior is explained by the increase in the electric field intensity associated with the voltage increase, which generates stronger Coulomb forces on the polymer jet, promoting greater stretching and favoring the formation of thinner fibers of 17 μm (see Fig. 1a).[68,71,72] The Coulomb force induced by the charges in the jet acts against the surface tension with tries to maintain the cohesion of the liquid. As the voltage increases, the electrostatic and Coulomb forces dominate, stretching the jet and reducing the diameter of the fibers.[73] Previous studies have confirmed that higher voltage produces this more intense stretching force, which reduces the diameter of the fibers.[68,74,75] However, when certain limits are exceeded, as was the case in the present study with voltages close to 30 kV, the repulsive forces generated by the charge accumulation in the jet can lead to instabilities, commonly known as Rayleigh instabilities, in which the jet decreases in size due to the inability of the surface tension to counteract the charge repulsion.[32,76] On the other hand, the type of collector and its configuration also play an important role in the morphology of the ultrathin fibers. Both static and a rotating collector were used, evaluating rotational speeds up to 600 rpm. The results demonstrate that as the collector speed increased from 0 to 600 rpm, the average fibre diameter decreased from 0.51 μm to 0.32 μm (Fig. 1b). This behavior is consistent with previous studies, which report that rotating collectors promote fiber alignment and enhance the stretching of the solution jet, resulting in a reduction in fiber diameter.[77,78] This trend is further supported by the diffraction patterns (Fig. 1b.iv, 2b.v, and 1b.vi), where the higher intensity indicates a predominant fibre orientation. These patterns confirm that the electrospun fibers exhibit a well-defined orientation along a specific axis as the collector speed increases. In addition, it was observed that the fiber diameter was slightly smaller (0.49 μm) in the vertical configuration compared to the horizontal configuration (0.51 μm).[79,80] This result is related to the additional influence of gravity in the vertical configuration, which favors the stretching of the solution jet.[80] Finally, the environmental conditions of the electrospinning process have been studied, especially the effect of humidity. It is observed that by decreasing the relative humidity from 45% to 25% and increasing it to

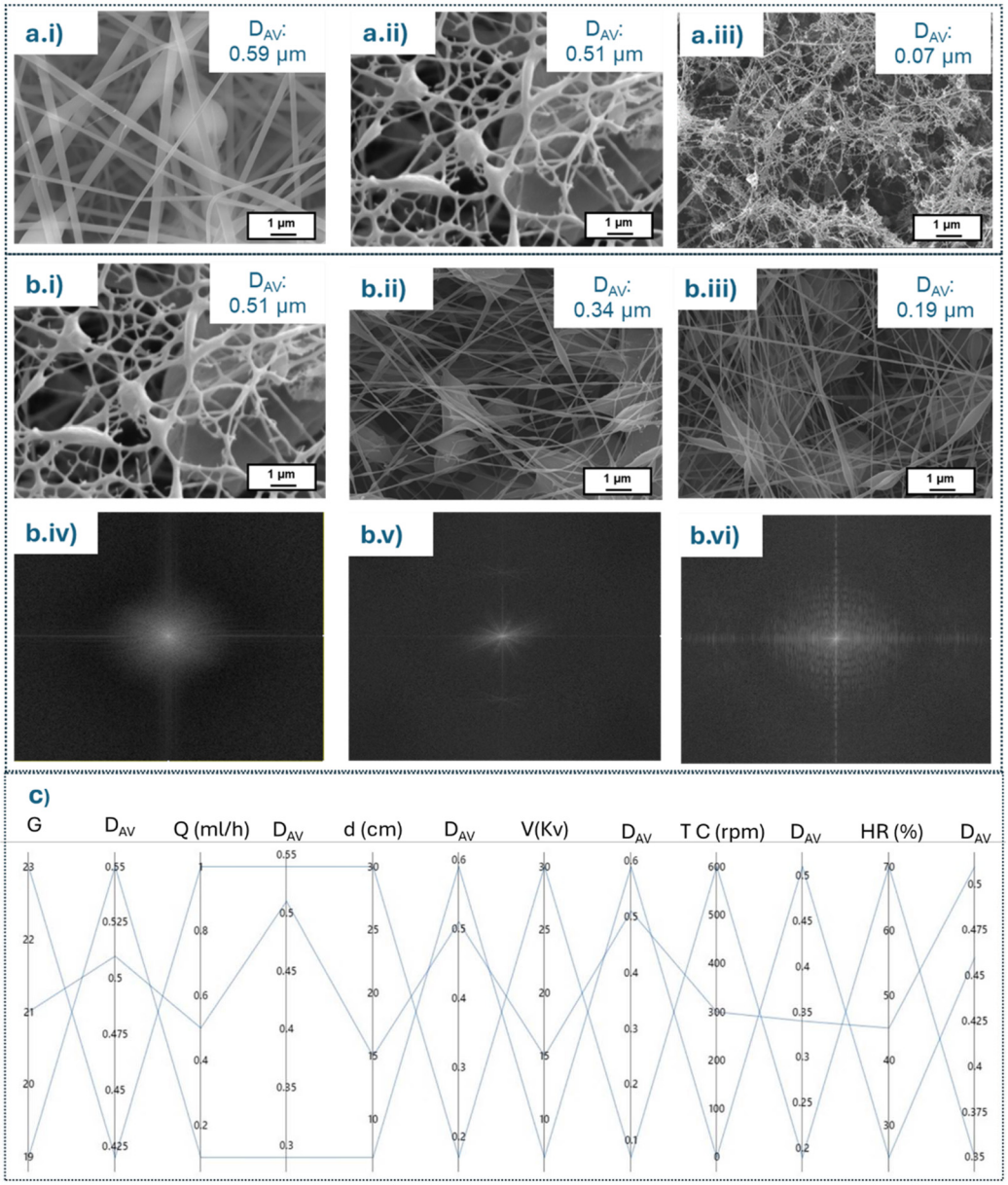

Fig. 1 SEM micrographs of electrospun nanostructures from the 90LSL-10PCL spinning solution under different conditions: (a) Applied voltages: (i) 7 kV, (ii) 15 kV, and (iii) 30 kV. (b) Effect of collector rotation speed on SEM morphologies and diffraction patterns for: (i) 0 rpm, (ii) 300 rpm, (iii) 600 rpm, (iv) 0 rpm, (v) 300 rpm, and (vi) 600 rpm. (c) Parallel axis plot showing the different electrospinning conditions and their effect on the average fiber diameter.

70%, the D_{AV} of the nanostructures decreases by 0.46 and 0.35 µm, respectively. This phenomenon highlights the sensitivity of the electrospinning process to environmental conditions, as it directly affects the evaporation of the solvent and the formation of the Taylor cone.[38,81]

Based on the results obtained during the study of the processing conditions, the following electrospinning parameters were selected as reference for the subsequent tests: a 21*G* needle gauge, a flow rate of 0.5 ml h^{-1}, an applied voltage of 15 kV, relative humidity 45% and a static collector using a horizontal configuration. These key parameters were chosen for their ability to produce fibers with uniform morphology and optimal diameter, while maintaining beam stability and process reproducibility.

2.2. Influence of physicochemical properties of LSL/PCL spinning solutions on the electrospun nanostructures

Numerous studies have shown a significant correlation between electrospinnability and physicochemical properties of spinning solutions, such as dynamic viscosity, surface tension and electrical conductivity.[25,82–84] These properties are determined by factors such as the type of polymer, its molecular weight, the solvent used, and the concentration of the polymer

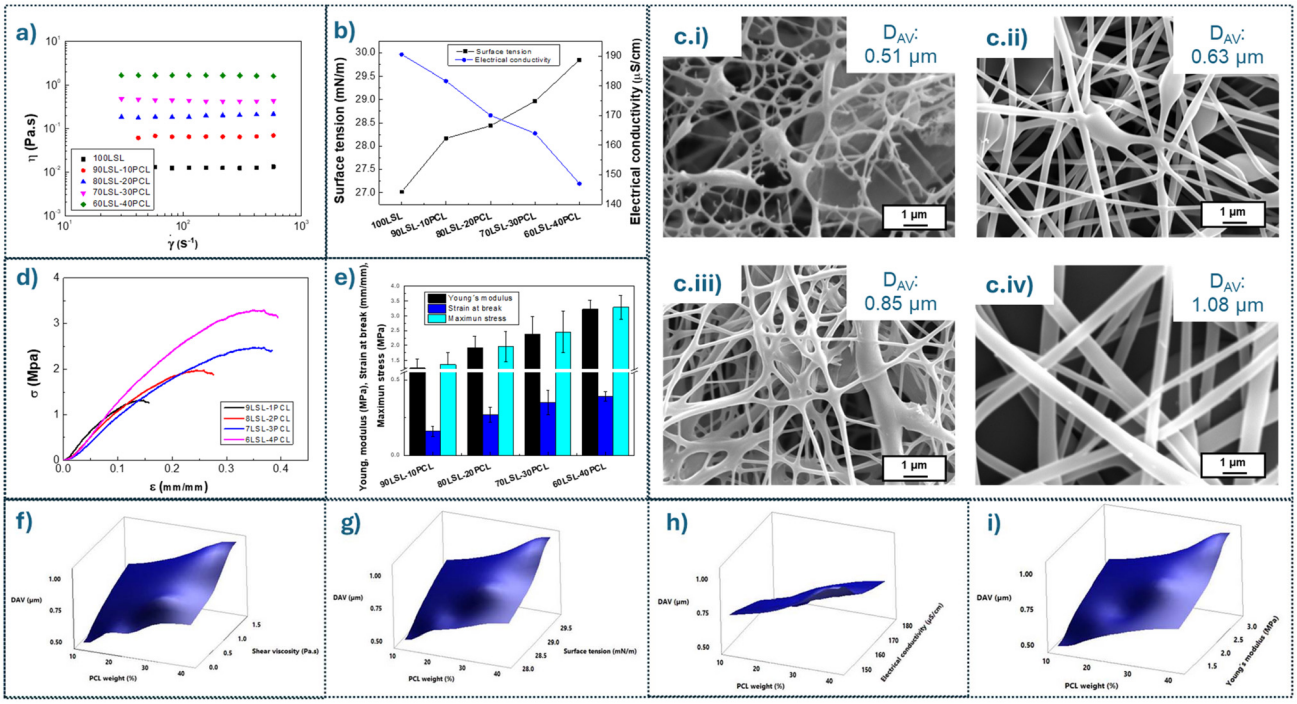

Fig. 2 (a) Viscous flow curves; (b) surface tension and electrical conductivity for spinning solutions with different ratios of LSL/PCL; (c) SEM micrographs of electrospun nanostructures for: (i) 90LSL-10PCL, (ii) 80LSL-20PCL, (iii) 70LSL-30PCL and, (iv) 60LSL-40PCL; (d, e) mechanical properties of electrospun nanostrutures; and 3D mapping relating PCL weight, DAV and: (f) shear viscosity; (g) surface tension; (h) electrical conductivity; and (i) Young's modulus.

in solution.[24,85] Fig. 2a shows the relationship between dynamic viscosity and shear rate for different concentrations of LSL spinning solutions with different LSL/PCL ratios in a DMF/Chl (1 : 2) solvent mixture. All solutions evaluated showed Newtonian behavior in the shear rate range studied, with an increase in viscosity observed as the PCL content in the LSL/PCL mixture increased. This phenomenon is due to the higher molecular weight of PCL, which directly affects dynamic viscosity. These results are consistent with previous studies,[48,54,86] such as those of Ahn *et al.*,[87] who investigated the effect of lignin content on the electrospinning of cellulose solutions and its influence on the rheological properties of the spinning solutions and the morphologies of the produced fibers. The results showed that solutions with lower lignin content had higher viscosities and facilitated a more stable electrospinning process.

Fig. 2b shows the evolution of surface tension and electrical conductivity in spinning solutions with different LSL/PCL ratios. It can be observed that the surface tension does not show significant variations. In the solution with 100LSL, the surface tension is about 27.02 mN m^{-1}, which increases to 29.95 mN m^{-1} when the PCL ratio reaches 40 wt% (60LSL-40 PCL). This slight increase in surface tension can be attributed to the higher intermolecular cohesion between the PCL chains,[88] which implies a higher surface resistance of the solution, a common phenomenon in higher molecular weight polymers.[49,89] On the other hand, electrical conductivity decreases significantly with increasing PCL content. The solution with 100LSL shows a conductivity of 190.5 μS cm^{-1}, which decreases to 145.2 μS cm^{-1} in the solution with 60LSL-40PCL. This decrease in conductivity is related to the increase in viscosity, which reduces the mobility of charged species in the solution, thus limiting charge transport.[83,90]

Fig. 2c shows the morphological properties of electrospun mats from LSL/PCL solutions. The electrospinning process failed to produce fibers without the addition of a minimal amount of PCL; in its absence, mainly submicron electrospun particles were formed.[25,54,83] However, the addition of 10 wt% PCL to the LSL/PCL mixture promoted the formation of isolated filaments connecting micrometer particles (Fig. 2c.i). This effect was enhanced at a ratio of 80LSL-20PCL (Fig. 2c.ii), where the higher PCL content induced an increase in the D_{AV} of nanofiber network, which partially embedded the microparticles. The increased PCL content in the LSL/PCL blend directly affected both the mean fiber diameter and the structural heterogeneity, as shown in Fig. 2c.iii and c.iv, where the mean fiber diameter increased from 0.85 to 1.08 μm in the 70LSL-30PCL and 60LSL-40PCL systems, respectively. These results are attributed to the effect of PCL on the physicochemical properties of the spinning solution. The contribution of the physicochemical properties of the solutions can be seen in Fig. 2f, g and h, which show the influence of dynamic viscosity under shear, surface tension and electrical conductivity on D_{AV}. These results are con-

sistent with previous studies,[50,91] which emphasize the importance of incorporating a minimum amount of dopant polymer to achieve a certain entanglement concentration and thus obtain uniform and defect-free lignin nanofibers during the electrospinning process.[92–94]

Fig. 2d shows the stress–strain curves of electrospun meshes with different LSL/PCL ratios. All curves show similar mechanical behavior, which can be divided into three phases: an initial linear region, indicating an elastic response; then a decrease in slope, corresponding to the plastic phase, in which the deformation continues to increase; finally, each curve reaches a maximum stress followed by an abrupt decrease, indicating the breaking point of the material. It is observed that as the PCL content in the samples increases, the maximum strain before fracture increases, indicating higher mechanical strength. In particular, the sample with the highest PCL content (6LSL-4PCL) has a maximum stress close to 3.5 MPa, while the sample with the lowest PCL content (9LSL-1PCL) reaches approximately 1.5 MPa. Similarly, the maximum elongation at break also increases with the PCL content, suggesting a higher ductility in the fibers with higher amounts of this polymer. The mechanical parameters are tabulated in Fig. 2e. This increase in the mechanical properties of the electrospun meshes with increasing PCL content was predictable due to two factors: (i) PCL, as a synthetic polymer, exhibits superior mechanical performance compared to natural polymers; and (ii) the structural properties of the electrospun nanostructures, which become more uniform, defect-free and larger in diameter with increasing PCL content,[35,95] as shown in the 3D mapping in Fig. 2i.

2.3. Exploration of electrospinning conditions and physicochemical parameters on the properties of oleo-dispersions

Previous studies have shown that electrospun nanostructures consisting of well-defined nanofiber meshes or beaded nanofibers connecting microparticles and/or nanoparticles are capable of forming stable gel-like systems when dispersed in vegetable oil.[27,52] In contrast, nanostructures formed by electrospraying produce unstable dispersions that cause oil separation.[52,96] This difference is attributed to the fact that nanofibers provide greater stabilization through a combination of physical interactions. The hydrophobic nature of PCL increases its affinity for the castor oil phase,[25,97] while the hydrophilic functional groups of lignin, such as hydroxyl groups, allow hydrogen bonding with the ricinoleic acid in castor oil, further contributing to the stabilization of the system.[98,99] In addition, van der Waals forces play an important role due to the high surface area-to-volume ratio of the electrospun nanofibers, which enhances their contact and interaction with the oil phase, while π–π stacking interactions due to the aromatic regions in lignin, although present, contribute to the stabilization to a lesser extent.[100,101] These interactions allow the oil to be trapped within the three-dimensional network, facilitating its diffusion through the nanostructure and acting as a scaffold for oleo-dispersion.[89,102] Fig. 3a.i shows a three-dimensional reconstruction by confocal microscopy of the oleo-dispersion prepared with the 90LSL-10PCL nanostructure electrospun under optimized conditions (Fig. 2c.i) and selected as a reference. It was observed that the homogeneous dispersion of nanofibers does not significantly alter their morphology. However, it is worth noting the remarkable swelling they undergo when dispersed in oil, which leads to a significant increase in the diameter of the fibers and particles within the percolation network. Fig. 3a.ii evaluates the influence of the thickener content in the reference nanostructure on the mechanical spectra of the oleo-dispersions obtained from Small-amplitude oscillatory shear (SAOS) tests in the linear viscoelastic range. The viscoelastic behavior was qualitatively similar among the samples tested. The storage modulus (G') was higher than the loss modulus (G'') throughout the frequency range studied, although both showed different trends as a function of frequency. It was observed that the values of G' and G'' increased with increasing thickener concentration, indicating an increase in fiber density within the percolation network, probably due to compaction effects.[103] The profiles and values of the SAOS functions are very similar to those of conventional NLGI 2 lithium greases, particularly O-9LSL-1PCL_15 wt%.[13,15] In addition, the loss tangent (tan (δ) = G''/G'), remained unaffected over the entire frequency range, indicating that the thickener content does not impact the relative elasticity of the oleo-dispersion. To illustrate the effect of thickener content on the viscoelastic response of the oleo-dispersions, the plateau modulus (G_N^0) as defined elsewhere,[104] was plotted as a function of thickener content in Fig. 3a.iii and compared to that of a conventional lithium grease. The results show that renewable oleo-dispersions based on electrospun nanostructures require a lower amount of thickener to obtain viscoelastic properties similar to those of conventional greases, showing an exponential evolution in both cases.

Fig. 3b shows the variation of the SAOS functions for the lubricating oleo-dispersions prepared with the 90LSL-10PCL nanostructure under different electrospinning conditions, maintaining a fixed thickener content of 15 wt%. It is observed that for all the oleo-dispersions, regardless of the electrospinning processing conditions, the G' is higher than the G'' over the whole frequency range studied. This indicates that the oleo-dispersions maintain a predominantly elastic behavior, which is characteristic of systems with well-structured three-dimensional networks capable of storing elastic strain energy.[96,105] The electrospinning conditions play a critical role in the viscoelastic response of the system. Structures formed by homogeneous and larger diameter micro and/or nanofibers exhibit higher values of both G' and G'', suggesting that three-dimensional networks formed by higher diameter nanofibers are more efficient, increasing the stability of the system and conferring greater stiffness.[54,96] This translates into a greater capacity for elastic energy storage under small loads. On the other hand, as the size of the fibers decreases and the nanostructures become more heterogeneous, the values of G' and

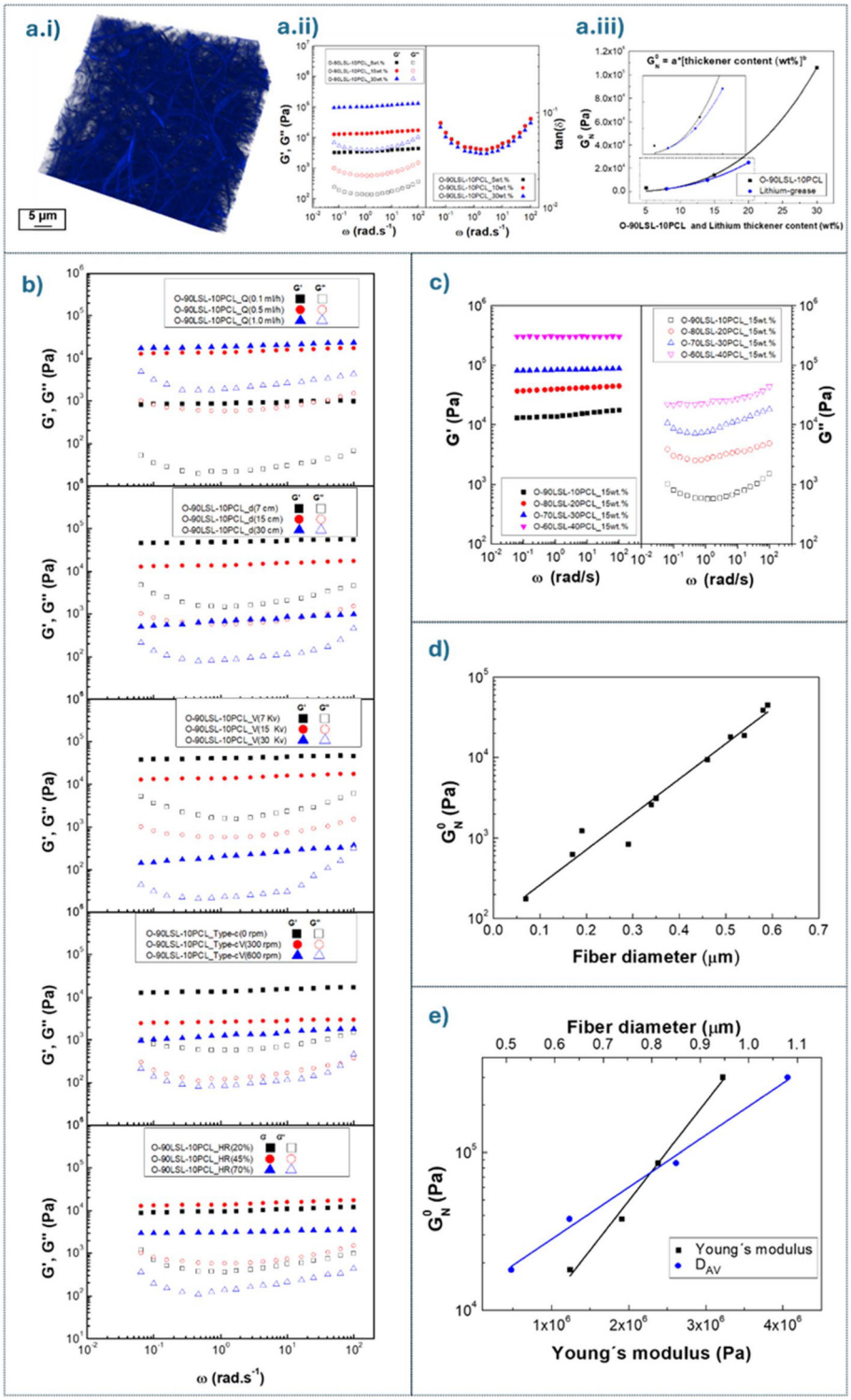

Fig. 3 (a.i) 3D reconstruction by confocal microscopy of O-90LSL-10PCL_15 wt%, (a.ii) frequency dependence of the *G*′ and *G*″, and loss tangent for the 90LSL-10PCL nanostructure at 5, 10, and 15 wt%, (a.iii) effect of thickening agent content on the linear viscoelastic response of O-90LSL-10PCL compared to conventional lithium lubricating grease; (b) dependence of *G*′ and *G*″ on frequency for the electrospun 90LSL-10PCL nanostructure-based oleo-dispersions, as a function of electrospinning process conditions; (c) dependence of *G*′ and *G*″, and loss tangent on frequency at different LSL/PCL weight ratios; (d) empirical correlation between fiber diameter and G_N^0 for different electrospinning conditions; and (e) empirical correlation between maximum strain and Young's modulus with G_N^0 for different LSL/PCL ratios.

G'' are reduced, decreasing the separation between the two modules, reflecting a decrease in the elastic character of the material and a more fluid behavior. These results are consistent with previous studies and indicate that the rheological properties depend on the electrospun nanostructure.[27,82] For instance, Valoppi *et al.*[26] reported similar trends in viscoelasticity for electrospun nanostructures, with a noticeable impact of fiber diameter on the G' and G'' values. However, our study is the first to systematically modulate these properties through electrospinning conditions, revealing a novel approach for improving the rheological behavior of oleo-dispersions with renewable materials. Furthermore, the observed behavior aligns with findings by Borrego *et al.*,[106] who noted that smaller fibers reduce the viscoelastic properties of similar systems, but our work offers new insights into how electrospinning parameters can be optimized to enhance the stability and performance of lubricating oleo-dispersions.

Fig. 3d illustrates this phenomenon by showing the relationship between the G_N^0 and the fiber diameter obtained in the different electrospun nanostructures under different conditions. A direct and linear relationship is observed between this viscoelastic modulus of the oleo-dispersions and D_{AV} of the electrospun nanostructures, which act as a scaffold in these gel-like dispersions.

Fig. 3c shows the variation of the SAOS functions for the oleo-dispersions prepared with the nanostructures (optimized electrospinning conditions) by varying the LSL/PCL ratio. The rheological response was consistent over the whole frequency range studied; however, both G' and G'' decreased significantly with increasing the LSL/PCL ratio. This behavior could be

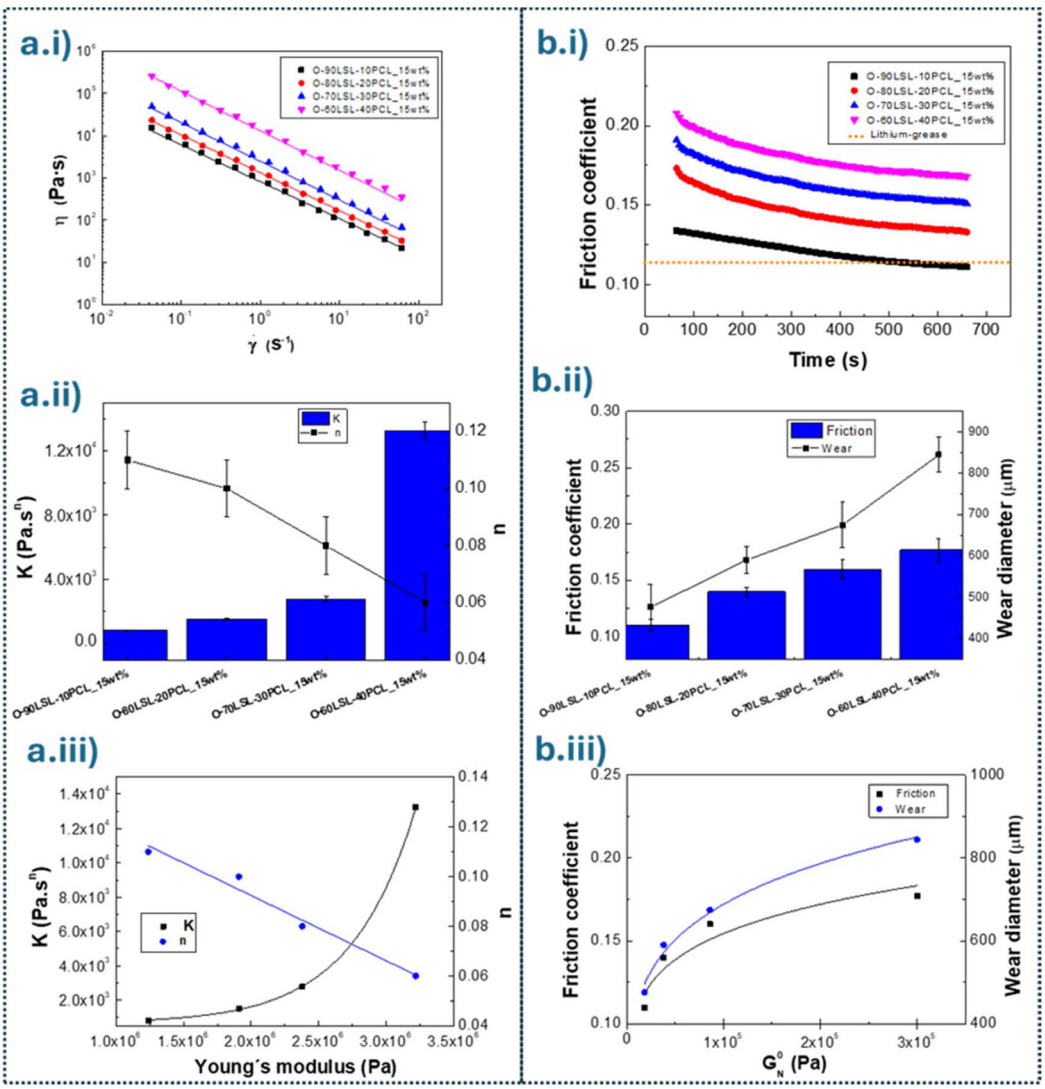

Fig. 4 (a.i) Evolution of viscosity as a function of shear rate, (a.ii) histogram with tabulated values of consistency (K) and flow (n) indices, (a.iii) empirical correlation between K and n with the Young's modulus. (b.i) Friction coefficient as a function of time, (b.ii) histogram with tabulated values of friction coefficients and wear track diameters, (b.iii) empirical correlation between friction coefficients and wear track diameters with G_N^0 for oleo-dispersions prepared with different LSL/PCL ratios.

related to: (i) an increase in the proportion of the lower molecular weight (LSL) component within the nanostructure, (ii) a negative effect on the morphological properties, such as the appearance of ultrathin fibers of smaller diameter and lower uniformity, as discussed above, and (iii) a reduction in the mechanical properties of the electrospun nanostructures.[86,106] These phenomena are interrelated as illustrated in Fig. 3e, which shows the relationship between G_N^0 and the Young's modulus of nanofibers, as well as average fiber size. In both cases, the viscoelastic moduli of the oleo-dispersions follow a linear trend, with a steeper slope relative to the mechanical properties. These, in turn, are correlated with the fiber diameter, as discussed above, and the results are in agreement with those obtained by other authors.[54,95]

2.4. Lubricating properties of structured oleo-dispersions based on electrospun LSL/PCL mats

Fig. 4 shows the viscous and tribological properties of oil dispersions structured with LSL/PCL electrospun mats in order to study their lubricating properties. Fig. 4a.i presents the viscous flow curves, where a shear thinning behavior following the power law model (eqn (1)) is observed,[82] showing a progressive decrease in viscosity with increasing shear rate ($\dot{\gamma}$).

$$\eta = K \cdot \dot{\gamma}^{n-1} \quad (1)$$

where K and n are the consistency and flow indices, respectively. Fig. 4a.ii shows the values of both fitting parameters for the different oleo-dispersions. Although the influence of the LSL weight ratio on the viscosity is minor, both K and n were also found to depend on the morphological properties of the electrospun nanostructures, which in turn are influenced by the LSL ratio. Fig. 4a.iii illustrates the trends of K and n as a function of Young's modulus. It is interesting to note that K varies exponentially with Young's modulus, while n depends linearly on these parameters within the observed experimental ranges. In general, K increased with higher PCL content, while the flow index decreased and remained relatively low in all cases, which is characteristic of materials with pronounced non-Newtonian properties, similar to conventional greases.[24,107]

Fig. 4b.i shows the tribological behavior of oleo-dispersions formulated with different LSL/PCL ratios, dispersed at a concentration of 15 wt%. The coefficients of friction decrease progressively throughout the test until they stabilize, indicating the formation of a stable lubricant film.[108,109] Fig. 4b.ii shows the tabulated values of both the coefficients of friction and the average diameter of the wear marks produced on the steel plates. Oleo-dispersions with higher concentrations of PCL show larger wear marks and higher coefficients of friction. In contrast, formulations with lower PCL concentrations show a progressive reduction in both coefficient of friction and track diameter. Oleo-dispersion O_90LSL-10PCL_15 wt% showed a remarkably low coefficient of friction and reduced wear footprint size, similar to the behavior observed in the lithium grease used as a reference. These results suggest that the three-dimensional nanofiber networks observed at higher LSL ratios retain oil more efficiently.[89,106] Moreover, as shown in Fig. S1.a,† the incorporation of LSL improves the thermal stability of the electrospun mats, exhibiting a higher decomposition onset temperature and higher residue content compared to neat PCL. In addition, DSC data reveal that the incorporation of LSL causes an increase in the T_g of the electrospun nanostructure (see Fig. S1.b†), which falls within the temperature range of lubricating greases.[110] In particular, the friction coefficients and wear footprint size obtained with the O_90LSL-10PCL_15 wt% system were lower than those reported for lubricating oleogels developed by chemical interactions by other authors,[111–113] and comparable to the values observed in oleo-dispersions based on physical interactions in previous works.[27,89,95]

This highlights the effectiveness of the proposed formulation in achieving favorable tribological properties without resorting to a complex chemical structuring method. Furthermore, as shown in Fig. 4b.iii, the softer rheological response of these gelled dispersions may have contributed to better penetration of the thickener into the tribological contact zone. This is reflected in the fact that both the coefficient of friction and the wear track diameter may increase with G_N^0, with the track diameter showing.

3. Concluding remarks

This study presents an innovative approach for the preparation of lubricating oleo-dispersions with electrospun nanofibers by varying the electrospinning parameters, which allows the modification of the system properties without changing its chemical composition. This is the first work where the properties of oleo-dispersions are systematically modulated through electrospinning processing conditions, such as applied voltage, collector configuration, and LSL/PCL component ratio. It has been demonstrated that small adjustments in processing conditions, such as applied voltage, collector configuration and LSL/PCL component ratio, significantly affect the rheological and tribological properties.

It was observed that increasing the applied voltage and modifying the collector configuration resulted in electrospun ultrathin fibers exhibiting a reduction in diameter and an improvement in homogeneity. The morphological modification, achieved solely by optimizing the processing conditions, resulted in oleo-dispersions with improved SAOS functions. Regarding the mechanical properties of the membranes, it was found that variations in the LSL/PCL ratio had a direct effect on their stiffness and wear resistance. Oleo-dispersions with a higher PCL content showed increased stiffness, which was reflected in an increase of the SAOS functions within the mechanical spectrum. However, this was also accompanied by an increase in the coefficient of friction and the size of the wear marks due to the formation of stiffer and more robust structures that, while providing greater mechanical stability, increase friction in the tribological contact.

This work not only provides a deep understanding of the relationship between electrospinning conditions and the properties of oleo-dispersions, but also provides a flexible platform for the development of renewable and customizable lubricants. The results suggest that it is possible to create oleo-dispersions with tailored properties for specific applications by simply modifying the electrospinning parameters, thus providing a promising route for the design of sustainable and high-performance lubricants. However, future work is needed to explore the use of sustainable and renewable solvents in the formulation of these systems. Additionally, tribological testing under different conditions, as well as technological testing to simulate real-world applicability conditions, will be required to further optimize the design and performance of these lubricants in operational environments.

4. Materials and methods

4.1. Materials

Commercial softwood low-sulfonate Kraft lignin (LSL, M_w: ~10 000 g mol^{-1}) and polycaprolactone (PCL, M_w: 80 000 g mol^{-1}) were obtained from Merck Sigma-Aldrich. *N*,*N*-Dimethylformamide (DMF) and chloroform (Chl), also acquired from Merck Sigma-Aldrich (Darmstadt, Germany), were used as solvents. Castor oil was purchased from Guinama (Valencia, Spain). The fatty acid composition and primary physical properties of this vegetable oil are described in detail in another publication.[114]

4.2. Preparation and characterization of LSL/PCL solutions

Spinning solutions were prepared at 20 wt% and with different LSL/PCL wt% ratios (see Table 2). A solvent mixture of DMF/Chl (1 : 2 v/v) was used for the preparation. The process involved stirring with a magnetic stirrer at 650 rpm for 24 hours at room temperature (22 °C).

LSL and LSL/PCL spinning solutions underwent physicochemical characterization, starting with the measurement of dynamic shear viscosity, followed by surface tension, and finally electrical conductivity. The tests were conducted at room temperature. Shear viscosity measurements for the LSL and LSL/PCL solutions were performed using a strain-controlled rotational rheometer (ARES Rheometric Scientific, UK) equipped with coaxial cylinders (inner diameter: 32 mm, length: 33.35 mm, gap: 1 mm), applying a shear rate ramp ranging from 0.02 to 600 s^{-1}. Surface tension was determined using a surface tensiometer (Sigma 703D, Biolin Scientific, China) with a platinum Wilhelmy plate (39.24 mm wide × 0.1 mm thick). Finally, electrical conductivity was measured using a conductivity meter (GLP 31, Crison, Spain) equipped with an immersion cell, calibrated with standard KCl solutions within the appropriate concentration range. All tests were performed in triplicate.

Table 2 Codification and ratios for LSL/PCL spinning solutions (wt/wt)

Sample code	LSL (wt%)	PCL (wt%)
100LSL	100	0
90LSL-10PCL	90	10
80LSL-20PCL	80	20
70LSL-30PCL	70	30
60LSL-40PCL	60	40

4.3. Electrospinning and characterization of LSL and LSL/PCL electrospun mats

Electrospinning process of the spinning solutions was performed in an electrospinning chamber from Inovenso (NS24, Turkey). First, a study of the electrospinning conditions was carried out using the 90LSL-10PCL solution, which was placed in a 10 mL syringe connected to an infusion pump that regulated the flow rate between 0.1 and 1 mL h^{-1}. Both horizontal and vertical configurations were established, with distances of 7 to 30 cm between the collection plate and the needle tip (dimensions used: 19, 21, and 23*G*). Electrical connections were made between the collection plate, the capillary and a high voltage power supply, generating a potential difference of 7 to 30 kV. Experiments were performed at room temperature with controlled relative humidities of 20–70 ± 1%.

The morphology of the electrospun nanostructures was investigated by scanning electron microscopy (SEM) using a JXA-8200 SuperProbe microscope (JEOL Ltd, Japan) equipped with a secondary electron detector operating at an acceleration voltage of 15 kV. Due to their chemical composition, the samples exhibited limited conductivity, which required prior gold sputtering using a BTT150 sputter coater (HHV, UK).[115] SEM micrographs analysis was performed with the open source software FIJI ImageJ, using a specialized plug-in called DiameterJ.[116] The mechanical properties of the nanostructures were determined by uniaxial tensile tests using a universal testing machine (Shimadzu Corporation, Kyoto, Japan) equipped with a 50 N load cell. The tests were performed at a strain rate of 0.1 mm s^{-1}. Rectangular specimens of 12.5 × 30 mm (~0.5 mm width) were prepared and fixed in metal clamps lined with sandpaper to prevent slippage or premature fracture. Mechanical properties, including peak stress, strain at break, and Young's modulus, were measured and analyzed.

Thermogravimetric analysis (TGA) of LSL, PCL and electrospun nanostructure was conducted under N_2 using a Q-50 analyzer (TA Instruments, USA). Samples (4–7 mg) were heated from 30 to 600 °C at a rate of 10 °C min^{-1} in platinum pans. Differential scanning calorimetry (DSC) was performed with a Q100 calorimeter (TA Instruments, USA) following a heating–cooling–heating cycle from −75 to 220 °C at 10 °C min^{-1} to eliminate thermal history. Samples (5–10 mg) were sealed in aluminum pans and purged with N_2 at 50 mL min^{-1}. The glass transition temperatures (T_g) were calculated from the calorimetric data obtained during the second heating ramp.

4.4. Preparation and characterization of LSL/PCL oleo-dispersions

The electrospun LSL/PCL nanostructures were carefully removed from the collector plate using tweezers and a spatula.

Selected nanostructures were dispersed in castor oil at concentrations of 5, 15, and 30 wt% using an IKA RW-20 mixer (IKA, Germany) equipped with a low-shear anchor impeller. Oleo-dispersions were obtained by following a protocol of 60 rpm rotational speed for 24 hours at room temperature.[96] Afterward, the resulting oleo-dispersions were left to rest for an additional 24 hours prior to further characterization.

Rheological analysis of the oleo-dispersions was conducted at 25 °C using a controlled-stress rheometer Rheoscope (ThermoHaake, Germany). To minimize slippage, a rough plate-and-plate configuration was employed (20 mm plate diameter, 1 mm gap, 0.4 relative roughness). Small-amplitude oscillatory shear (SAOS) tests were performed within the linear viscoelastic region, covering a frequency range of 0.03 to 100 rad s^{-1}. Additionally, viscous flow behavior was assessed across shear rates ranging from 0.01 to 100 s^{-1}. Tribological tests were carried out using a Physica MCR-501 rheometer (Anton Paar, Graz, Austria), equipped with a tribology cell. The cell configuration included a steel ball with a 6.35 mm diameter (1.4401 Grade 100 AISI 316, roughness = 0.10 μm, Rockwell B-scale hardness = 79 HRB), which rotated against three rectangular steel plates inclined at 45° (1.4301 AISI 304, roughness = 0.21 μm, Rockwell B-scale hardness = 80 HRB). The oleo-dispersions samples, serving as lubricants, were applied on the plates. The tests were conducted under a constant normal load of 20 N, with a rotational speed of 10 rpm, for a duration of 10 minutes. Normal forces and friction coefficients were determined from the axial force and torque measured by the rheometer, following the method described by Heyer and Läuger[117] for this specific setup. The morphology of the oleo-dispersions was further examined using a Leica Stellaris 8 Falcon confocal laser scanning microscope equipped with Leica HCX PL APO lambda blue 63× 1.4 hybrid oil objectives was used. The AOBS-free spectral detection ranged from 410 to 850 nm.

4.5. Statistical analysis

Statistical analysis was performed on all evaluated parameters using one-way analysis of variance (ANOVA) with three independent replicates for each measurement. This approach allowed the calculation of key statistical measures such as mean and standard deviation. In addition, a *post-hoc* test was performed to determine significant differences between means, with a significance level of $p < 0.05$.

Author contributions

José F. Rubio-Valle: writing – original draft, software, methodology, investigation, formal analysis, data curation, conceptualization. Concepción Valencia: writing – review & editing, visualization, resources, formal analysis, data curation, investigation. Gethzemani M. Estrada-Villegas: validation, data curation, investigation, resources. José E. Martín-Alfonso: visualization, validation, resources, formal analysis, investigation, writing – review & editing. José M. Franco: writing – review & editing, visualization, validation, supervision, resources, project administration, methodology, funding acquisition, investigation.

Data availability

The data supporting this article have been included as part of the article.

Conflicts of interest

The authors declare no conflict of interests.

Acknowledgements

This work is part of the Research Project PID2021-125637OB-I00, funded by MICIU/AEI/10.13039/501100011033 and by ERDF/EU. J. F. Rubio-Valle additionally received a PhD Research Grant PRE2019-090632 from Spain's Ministry of Science and Innovation. Funding is gratefully acknowledged.

References

1 L. Staffas, M. Gustavsson and K. McCormick, *Sustainability*, 2013, **5**, 2751–2769, DOI: **10.3390/su5062751**.
2 A. Aguilar, T. Twardowski and R. Wohlgemuth, *Biotechnol. J.*, 2019, **14**, DOI: **10.1002/biot.201800638**.
3 J. S. Damtoft, J. Lukasik, D. Herfort, D. Sorrentino and E. M. Gartner, *Cem. Concr. Res.*, 2008, **38**, 115–127, DOI: **10.1016/j.cemconres.2007.09.008**.
4 P. Friedlingstein and S. Solomon, *Proc. Natl. Acad. Sci. U. S. A.*, 2005, **102**, 10832–10836, DOI: **10.1073/pnas.0504755102**.
5 S. van Renssen, *Nat. Clim. Change*, 2014, **4**, 951–953, DOI: **10.1038/nclimate2419**.
6 M. Lainez, J. M. González, A. Aguilar and C. Vela, *Nat. Biotechnol.*, 2018, **40**, 87–95, DOI: **10.1016/j.nbt.2017.05.006**.
7 J. Elkington, *Environ. Qual. Manage.*, 1998, **8**, 37–51, DOI: **10.1002/tqem.3310080106**.
8 M. Bellini, S. Bianchi, F. Zaccheria and N. Ravasio, *Tribol. Int.*, 2021, **161**, 107103, DOI: **10.1016/j.triboint.2021.107103**.
9 Y. Li, F. Zambrano, Y. Wang and R. Marquez, *BioResources*, 2022, **17**, 3178–3201, DOI: **10.15376/biores.17.2.3178-3201**.
10 V. Shanmugam, O. Das, R. E. Neisiany, K. Babu, S. Singh, M. S. Hedenqvist, F. Berto and S. Ramakrishna, *Mater. Circ. Econ.*, 2020, **2**, 11, DOI: **10.1007/s42824-020-00012-0**.
11 A. Z. Syahir, N. W. M. Zulkifli, H. H. Masjuki, M. A. Kalam, A. Alabdulkarem, M. Gulzar, L. S. Khuong and M. H. Harith, *J. Cleaner Prod.*, 2017, **168**, 997–1016, DOI: **10.1016/j.jclepro.2017.09.106**.

12 R. Mas and A. Magnin, *J. Rheol.*, 1994, **38**, 889–908, DOI: 10.1122/1.550598.
13 Y. Wang, X. Gao, J. Lin and P. Zhang, *Lubricants*, 2022, **10**, 57, DOI: 10.3390/lubricants10040057.
14 M. B. Chittick, in *Evaluation of Petroleum Products*, ASTM International, 100 Barr Harbor Drive, PO Box C700, West Conshohocken, PA 19428–2959, 1940, pp. 11–18. DOI: 10.1520/STP47839S.
15 National Lubricating Grease Institute, *NLGI Lubricating Greases Guide*, Kansas City, MO, USA, 5th edn., 2006.
16 R. Narayana Sarma and R. Vinu, *Lubricants*, 2022, **10**, 70, DOI: 10.3390/lubricants10040070.
17 M. Bilal, S. A. Qamar, M. Qamar, V. Yadav, M. J. Taherzadeh, S. S. Lam and H. M. N. Iqbal, *Biomass Convers. Biorefin.*, 2024, **14**, 4457–4483, DOI: 10.1007/s13399-022-02600-3.
18 N. Salih and J. Salimon, *Biointerface Res. Appl. Chem.*, 2021, **11**, 13303–13327, DOI: 10.33263/BRIAC115.1330313327.
19 P. Ghosh, M. Hoque, G. Karmakar and S. Yeasmin, *Curr. Environ. Eng.*, 2017, **4**, 197–206.
20 G. Karmakar, P. Ghosh and B. Sharma, *Lubricants*, 2017, **5**, 44, DOI: 10.3390/lubricants5040044.
21 M. Trejo-Cáceres, M. C. Sánchez and J. E. Martín-Alfonso, *Int. J. Biol. Macromol.*, 2023, **227**, 673–684, DOI: 10.1016/j.ijbiomac.2022.12.096.
22 J. E. Martín-Alfonso, N. Núñez, C. Valencia, J. M. Franco and M. J. Díaz, *J. Ind. Eng. Chem.*, 2011, **17**, 818–823, DOI: 10.1016/j.jiec.2011.09.003.
23 R. Sánchez, G. Alonso, C. Valencia and J. M. Franco, *Chem. Eng. Res. Des.*, 2015, **100**, 170–178, DOI: 10.1016/j.cherd.2015.05.022.
24 M. A. Martín-Alfonso, J. E. Martín-Alfonso, J. F. Rubio-Valle, J. P. Hinestroza and J. M. Franco, *Appl. Mater. Today*, 2024, **36**, 102030, DOI: 10.1016/j.apmt.2023.102030.
25 J. F. Rubio-Valle, C. Valencia, G. Ferraro, M. Carmen Sánchez, J. E. Martín-Alfonso and J. M. Franco, *J. Mol. Liq.*, 2024, **414**, 126248, DOI: 10.1016/j.molliq.2024.126248.
26 F. Valoppi, J. Schavikin, P. Lassila, I. Laidmäe, J. Heinämäki, S. Hietala, E. Haeggström and A. Salmi, *Food Struct.*, 2023, **37**, 100338, DOI: 10.1016/j.foostr.2023.100338.
27 J. F. Rubio-Valle, C. Valencia, M. Sánchez, J. E. Martín-Alfonso and J. M. Franco, *Cellulose*, 2023, **30**, 1553–1566, DOI: 10.1007/s10570-022-04963-2.
28 K. Shi and K. P. Giapis, *ACS Appl. Energy Mater.*, 2018, **1**, 296–300, DOI: 10.1021/acsaem.7b00227.
29 J. L. Hernandez, M.-A. Doan, R. Stoddard, H. M. VanBenschoten, S.-T. Chien, I. T. Suydam and K. A. Woodrow, *Front. Biomater. Sci.*, 2022, DOI: 10.3389/fbiom.2022.928537.
30 J. F. Rubio-Valle, M. Jiménez-Rosado, V. Perez-Puyana, A. Guerrero and A. Romero, in *Antimicrobial Textiles from Natural Resources*, Elsevier, 2021, pp. 589–618. DOI: 10.1016/B978-0-12-821485-5.00020-2.
31 B. Robb and B. Lennox, in *Electrospinning for Tissue Regeneration*, Elsevier, 2011, pp. 51–66. DOI: 10.1533/9780857092915.1.51.
32 M. M. Hohman, M. Shin, G. Rutledge and M. P. Brenner, *Phys. Fluids*, 2001, **13**, 2201–2220, DOI: 10.1063/1.1383791.
33 V. Jacobs, R. D. Anandjiwala and M. Maaza, *J. Appl. Polym. Sci.*, 2010, **115**, 3130–3136, DOI: 10.1002/app.31396.
34 G. K. Celep and K. Dincer, *Int. Polym. Process.*, 2017, **32**, 508–514, DOI: 10.3139/217.3411.
35 J. Xue, T. Wu, Y. Dai and Y. Xia, *Chem. Rev.*, 2019, **119**, 5298–5415, DOI: 10.1021/acs.chemrev.8b00593.
36 V. Pillay, C. Dott, Y. E. Choonara, C. Tyagi, L. Tomar, P. Kumar, L. C. du Toit and V. M. K. Ndesendo, *J. Nanomater.*, 2013, **2013**, 1–22, DOI: 10.1155/2013/789289.
37 J. Lasprilla-Botero, M. Álvarez-Láinez and J. M. Lagaron, *Mater. Today Commun.*, 2018, **14**, 1–9, DOI: 10.1016/j.mtcomm.2017.12.003.
38 P. K. Szewczyk and U. Stachewicz, *Adv. Colloid Interface Sci.*, 2020, **286**, 102315, DOI: 10.1016/j.cis.2020.102315.
39 S. De Vrieze, T. Van Camp, A. Nelvig, B. Hagström, P. Westbroek and K. De Clerck, *J. Mater. Sci.*, 2009, **44**, 1357–1362, DOI: 10.1007/s10853-008-3010-6.
40 S. Jang, Y. Kim, S. Lee and J. H. Oh, *Int. J. Precis. Eng. Manuf. Technol.*, 2019, **6**, 731–739, DOI: 10.1007/s40684-019-00134-0.
41 J. Deitzel, J. Kleinmeyer, D. Harris and N. Beck Tan, *Polymer*, 2001, **42**, 261–272, DOI: 10.1016/S0032-3861(00)00250-0.
42 A. Naseem, S. Tabasum, K. M. Zia, M. Zuber, M. Ali and A. Noreen, *Int. J. Biol. Macromol.*, 2016, **93**, 296–313, DOI: 10.1016/j.ijbiomac.2016.08.030.
43 L. A. Zevallos Torres, A. Lorenci Woiciechowski, V. O. de Andrade Tanobe, S. G. Karp, L. C. Guimarães Lorenci, C. Faulds and C. R. Soccol, *J. Cleaner Prod.*, 2020, **263**, 121499, DOI: 10.1016/j.jclepro.2020.121499.
44 F. G. Calvo-Flores and J. A. Dobado, *ChemSusChem*, 2010, 3, 1227–1235. DOI: 10.1002/cssc.201000157.
45 A. M. Borrero-López, C. Valencia, D. Ibarra, I. Ballesteros and J. M. Franco, *Int. J. Biol. Macromol.*, 2022, **195**, 412–423, DOI: 10.1016/j.ijbiomac.2021.11.185.
46 R. Vanholme, B. Demedts, K. Morreel, J. Ralph and W. Boerjan, *Plant Physiol.*, 2010, **153**, 895–905, DOI: 10.1104/pp.110.155119.
47 Y. C. Lu, Y. Lu and X. Fan, in *Structure and Characteristics of Lignin*, ed. S. Sharma and A. Kumar, Springer Series on Polymer and Composite Materials, Springer, Cham, Switzerland, 2020, ch. 2, pp. 17–75, DOI: 10.1007/978-3-030-40663-9_2.
48 D. Ibarra, L. García-Fuentevilla, J. F. Rubio-Valle, R. Martín-Sampedro, C. Valencia and M. E. Eugenio, *React. Funct. Polym.*, 2023, **191**, 105685, DOI: 10.1016/j.reactfunctpolym.2023.105685.
49 J. F. Rubio-Valle, J. E. Martín-Alfonso, M. E. Eugenio, D. Ibarra, J. M. Oliva, P. Manzanares and C. Valencia, *Int. J. Biol. Macromol.*, 2024, **255**, 128042, DOI: 10.1016/j.ijbiomac.2023.128042.

50 I. Dallmeyer, L. T. Lin, Y. Li, F. Ko and J. F. Kadla, *Macromol. Mater. Eng.*, 2014, **299**, 540–551, DOI: 10.1002/mame.201300148.
51 E. Svinterikos, I. Zuburtikudis and M. Al-Marzouqi, *ACS Sustainable Chem. Eng.*, 2020, **8**, 13868–13893, DOI: 10.1021/acssuschemeng.0c03246.
52 J. F. Rubio-Valle, C. Valencia, J. E. Martín-Alfonso and J. M. Franco, *Ind. Crops Prod.*, 2024, **222**, 119442, DOI: 10.1016/j.indcrop.2024.119442.
53 J. Ruwoldt, *Surfaces*, 2020, **3**, 622–648, DOI: 10.3390/surfaces3040042.
54 M. Borrego, J. E. Martín-Alfonso, C. Valencia, M. C. Sánchez and J. M. Franco, *Polymers*, 2022, **14**, 4741, DOI: 10.3390/polym14214741.
55 S. Devadas, S. M. N. Al-Ajrash, D. A. Klosterman, K. M. Crosson, G. S. Crosson and E. S. Vasquez, *Polymers*, 2021, **13**, 992, DOI: 10.3390/polym13070992.
56 J. Wang, L. Tian, B. Luo, S. Ramakrishna, D. Kai, X. J. Loh, I. H. Yang, G. R. Deen and X. Mo, *Colloids Surf., B*, 2018, **169**, 356–365, DOI: 10.1016/j.colsurfb.2018.05.021.
57 J. M. Herdan, *Lubr. Sci.*, 1997, **9**, 161–172, DOI: 10.1002/ls.3010090205.
58 C. I. Betton, in *Chemistry and Technology of Lubricants*, Springer Netherlands, Dordrecht, 2009, pp. 435–457. DOI: 10.1023/b105569_15.
59 T. Subbiah, G. S. Bhat, R. W. Tock, S. Parameswaran and S. S. Ramkumar, *J. Appl. Polym. Sci.*, 2005, **96**, 557–569, DOI: 10.1002/app.21481.
60 F. Ding, H. Deng, Y. Du, X. Shi and Q. Wang, *Nanoscale*, 2014, **6**, 9477–9493, DOI: 10.1039/C4NR02814G.
61 S. Agarwal, J. H. Wendorff and A. Greiner, *Polymer*, 2008, **49**, 5603–5621, DOI: 10.1016/j.polymer.2008.09.014.
62 T. D. Stocco, N. J. Bassous, S. Zhao, A. E. C. Granato, T. J. Webster and A. O. Lobo, *Nanoscale*, 2018, **10**, 12228–12255, DOI: 10.1039/C8NR02002G.
63 S. Jang, Y. Kim, S. Lee and J. H. Oh, *Int. J. Precis. Eng. Manuf. Technol.*, 2019, **6**, 731–739, DOI: 10.1007/s40684-019-00134-0.
64 S. M. S. Shahabadi, A. Kheradmand, V. Montazeri and H. Ziaee, *Polym. Sci., Ser. A*, 2015, **57**, 155–167, DOI: 10.1134/S0965545X15020157.
65 D. H. Reneker and A. L. Yarin, *Polymer*, 2008, **49**, 2387–2425, DOI: 10.1016/j.polymer.2008.02.002.
66 M. E. Helgeson, K. N. Grammatikos, J. M. Deitzel and N. J. Wagner, *Polymer*, 2008, **49**, 2924–2936, DOI: 10.1016/j.polymer.2008.04.025.
67 A. Ahmadian, A. Shafiee, N. Aliahmad and M. Agarwal, *Textiles*, 2021, **1**, 206–226, DOI: 10.3390/textiles1020010.
68 Y. Yang, Z. Jia, J. Liu, Q. Li, L. Hou, L. Wang and Z. Guan, *J. Appl. Phys.*, 2008, **103**, DOI: 10.1063/1.2924439.
69 S. Lei, C. Xiong, Z. Quan, X. Qin and J. Yu, *Polymer*, 2021, **217**, 123443, DOI: 10.1016/j.polymer.2021.123443.
70 Z. Li and C. Wang, in *One-Dimensional Nanostructures*, Springer, Berlin, Heidelberg, 2013, ch. 2, pp. 15–28, DOI: 10.1007/978-3-642-36427-3_2.
71 W.-T. Kim, D.-C. Park, W.-H. Yang, C.-H. Cho and W.-Y. Choi, *Nanomaterials*, 2021, **11**, 1616, DOI: 10.3390/nano11061616.
72 G. Collins, J. Federici, Y. Imura and L. H. Catalani, *J. Appl. Phys.*, 2012, **111**, DOI: 10.1063/1.3682464.
73 K. Chen, J. Wu and A. L. Yarin, *J. Membr. Sci.*, 2022, **644**, 120138, DOI: 10.1016/j.memsci.2021.120138.
74 S. S. S. Bakar, K. C. Fong, A. Eleyas and M. F. M. Nazeri, *IOP Conf. Ser.:Mater. Sci. Eng.*, 2018, **318**, 012076, DOI: 10.1088/1757-899X/318/1/012076.
75 Y. Liu, L. Dong, J. Fan, R. Wang and J. Yu, *J. Appl. Polym. Sci.*, 2011, **120**, 592–598, DOI: 10.1002/app.33203.
76 T. Driessen, P. Sleutel, F. Dijksman, R. Jeurissen and D. Lohse, *J. Fluid Mech.*, 2014, **749**, 275–296, DOI: 10.1017/jfm.2014.178.
77 H. Yuan, Q. Zhou and Y. Zhang, in *Electrospun Nanofibers*, Elsevier, 2017, pp. 125–147. DOI: 10.1016/B978-0-08-100907-9.00006-4.
78 V. Perez-Puyana, M. Jiménez-Rosado, A. Guerrero and A. Romero, *Int. J. Fract.*, 2020, **224**, 269–276, DOI: 10.1007/s10704-020-00460-4.
79 D. Rodoplu and M. Mutlu, *J. Eng. Fibers Fabr.*, 2012, **7**, 155892501200700, DOI: 10.1177/155892501200700217.
80 S. Suresh, A. Becker and B. Glasmacher, *Polymers*, 2020, **12**, 2448, DOI: 10.3390/polym12112448.
81 Y. Cai and M. Gevelber, *J. Mater. Sci.*, 2013, **48**, 7812–7826, DOI: 10.1007/s10853-013-7544-x.
82 M. A. Martín-Alfonso, J. F. Rubio-Valle, G. M. Estrada-Villegas, M. Sánchez-Domínguez and J. E. Martín-Alfonso, *Gels*, 2024, **10**, 221, DOI: 10.3390/gels10040221.
83 J. F. Rubio-Valle, M. C. Sánchez, C. Valencia, J. E. Martín-Alfonso and J. M. Franco, *Polymers*, 2021, **13**, 2206, DOI: 10.3390/polym13132206.
84 S. L. Shenoy, W. D. Bates, H. L. Frisch and G. E. Wnek, *Polymer*, 2005, **46**, 3372–3384, DOI: 10.1016/j.polymer.2005.03.011.
85 P. Sánchez-Cid, J. F. Rubio-Valle, M. Jiménez-Rosado, V. Pérez-Puyana and A. Romero, *Polymers*, 2022, **14**, 665, DOI: 10.3390/polym14040665.
86 L. García-Fuentevilla, J. F. Rubio-Valle, R. Martín-Sampedro, C. Valencia, M. E. Eugenio and D. Ibarra, *Int. J. Biol. Macromol.*, 2022, **214**, 554–567, DOI: 10.1016/j.ijbiomac.2022.06.121.
87 Y. Ahn, Y. Kang, B. Park, M. K. Ku, S. H. Lee and H. Kim, *J. Appl. Polym. Sci.*, 2014, **131**, DOI: 10.1002/app.40031.
88 C. J. Luo, E. Stride and M. Edirisinghe, *Macromolecules*, 2012, **45**, 4669–4680, DOI: 10.1021/ma300656u.
89 J. F. Rubio-Valle, M. C. Sánchez, C. Valencia, J. E. Martín-Alfonso and J. M. Franco, *Ind. Crops Prod.*, 2022, **188**, 115579, DOI: 10.1016/j.indcrop.2022.115579.
90 M. A. Martín-Alfonso, J. F. Rubio-Valle, J. E. Martín-Alfonso and J. M. Franco, *Adv. Sustainable Syst.*, 2024, DOI: 10.1002/adsu.202300592.
91 H. Wu, C. Liu, Z. Jiang, Z. Yang, X. Mao, L. Wei and R. Sun, *Text. Res. J.*, 2022, **92**, 456–466, DOI: 10.1177/00405175211037191.

92 L. Kong and G. R. Ziegler, *Biomacromolecules*, 2012, **13**, 2247–2253, DOI: **10.1021/bm300396j**.
93 S. S. Ojha, M. Afshari, R. Kotek and R. E. Gorga, *J. Appl. Polym. Sci.*, 2008, **108**, 308–319, DOI: **10.1002/app.27655**.
94 D. Kong, M. Yang, X. Zhang, Z. Du, Q. Fu, X. Gao and J. Gong, *Macromol. Mater. Eng.*, 2021, **306**, DOI: **10.1002/mame.202100536**.
95 J. F. Rubio-Valle, C. Valencia, M. C. Sánchez, J. E. Martín-Alfonso and J. M. Franco, *Resour., Conserv. Recycl.*, 2023, **199**, 107261, DOI: **10.1016/j.resconrec.2023.107261**.
96 J. F. Rubio-Valle, C. Valencia, M. C. Sánchez-Carrillo, J. E. Martín-Alfonso and J. M. Franco, *ACS Sustainable Chem. Eng.*, 2024, **12**, 12260–12269, DOI: **10.1021/acssuschemeng.4c05013**.
97 D. Nguyen, M. Desse and C. Jegat, *Polymer*, 2022, **262**, 125442, DOI: **10.1016/j.polymer.2022.125442**.
98 L. Xu, Q. Yang, H. Liu, Q. Li, M. Li, X. Liu, S. Chen, X. Wang and H. Suo, *Mol. Catal.*, 2024, **568**, 114521, DOI: **10.1016/j.mcat.2024.114521**.
99 Y. L. Uscátegui, L. E. Díaz, J. A. Gómez-Tejedor, A. Vallés-Lluch, G. Vilariño-Feltrer, M. A. Serrano and M. F. Valero, *Molecules*, 2019, **24**, 237, DOI: **10.3390/molecules24020237**.
100 L. Lou, O. Osemwegie and S. S. Ramkumar, *Ind. Eng. Chem. Res.*, 2020, **59**, 5439–5455, DOI: **10.1021/acs.iecr.9b07066**.
101 Y. Sun, X. Zhang, M. Zhang, M. Ge, J. Wang, Y. Tang, Y. Zhang, J. Mi, W. Cai, Y. Lai and Y. Feng, *Chem. Eng. J.*, 2022, **446**, 137099, DOI: **10.1016/j.cej.2022.137099**.
102 M. Borrego, J. E. Martín-Alfonso, C. Valencia, M. del C. Sánchez Carrillo and J. M. Franco, *ACS Appl. Polym. Mater.*, 2022, **4**, 7217–7227, DOI: **10.1021/acsapm.2c01090**.
103 M. C. Sánchez, J. M. Franco, C. Valencia, C. Gallegos, F. Urquiola and R. Urchegui, *Tribol. Lett.*, 2011, **41**, 463–470, DOI: **10.1007/s11249-010-9734-x**.
104 J. D. Ferry, *Viscoelastic properties of polymers*, 1980. DOI: **10.1149/1.2428174**.
105 M. A. Martín-Alfonso, J. F. Rubio-Valle, J. P. Hinestroza, J. E. Martín-Alfonso and J. M. Franco, *Nano Mater. Sci.*, 2024, DOI: **10.1016/j.nanoms.2024.02.003**.
106 M. Borrego, J. E. Martín-Alfonso, M. C. Sánchez, C. Valencia and J. M. Franco, *Int. J. Biol. Macromol.*, 2021, **180**, 212–221, DOI: **10.1016/j.ijbiomac.2021.03.069**.
107 M. A. Delgado, M. C. Sánchez, C. Valencia, J. M. Franco and C. Gallegos, *Chem. Eng. Res. Des.*, 2005, **83**, 1085–1092, DOI: **10.1205/cherd.04311**.
108 P. Wen, Y. Lei, Q. Yan, Y. Han and M. Fan, *ACS Appl. Mater. Interfaces*, 2021, **13**, 11524–11534, DOI: **10.1021/acsami.1c00614**.
109 P. Wu, X. Chen, C. Zhang, J. Zhang, J. Luo and J. Zhang, *Friction*, 2021, **9**, 143–154, DOI: **10.1007/s40544-019-0359-2**.
110 G. Gow, in *Chemistry and Technology of Lubricants*, Springer Netherlands, Dordrecht, 2009, pp. 411–432. DOI: **10.1023/b105569_14**.
111 A. M. Borrero-López, C. Valencia, A. Blánquez, M. Hernández, M. E. Eugenio and J. M. Franco, *Polymers*, 2020, **12**, 2822, DOI: **10.3390/polym12122822**.
112 A. M. Borrero-López, R. Martín-Sampedro, D. Ibarra, C. Valencia, M. E. Eugenio and J. M. Franco, *Int. J. Biol. Macromol.*, 2020, **162**, 1398–1413, DOI: **10.1016/j.ijbiomac.2020.07.292**.
113 M. A. Delgado, E. Cortés-Triviño, C. Valencia and J. M. Franco, *Tribol. Int.*, 2020, **146**, 106231, DOI: **10.1016/j.triboint.2020.106231**.
114 L. A. Quinchia, M. A. Delgado, C. Valencia, J. M. Franco and C. Gallegos, *Ind. Crops Prod.*, 2010, **32**, 607–612, DOI: **10.1016/j.indcrop.2010.07.011**.
115 Stokroos, Kalicharan, Van Der Want and Jongebloed, *J. Microsc.*, 1998, **189**, 79–89, DOI: **10.1046/j.1365-2818.1998.00282.x**.
116 N. A. Hotaling, K. Bharti, H. Kriel and C. G. Simon, *Biomaterials*, 2015, **61**, 327–338, DOI: **10.1016/j.biomaterials.2015.05.015**.
117 P. Heyer and J. Läuger, *Lubr. Sci.*, 2009, **21**, 253–268, DOI: **10.1002/ls.88**.